International Journal of Thermofluid Science and Technology (2021)
Volume 8, Issue 4, Paper No. 080404
https://doi.org/10.36963/IJTST.2021080404
Research Article

Performance Enhancement of Centrifugal Pump through Cavitation Reduction using Optimization Techniques

Adnan Aslam Noon[1], Muhammad Arif[1], Javed Ahmed Khan Tipu[1], Absaar Ul Jabbar[2], Muftooh Ur Rehman Siddiqi[3,*], Aamer Sharif[4]

[1]Department of Mechanical Engineering, FET, International Islamic University, Islamabad, Pakistan
[2]National University of Sciences and Technology, Islamabad, Pakistan
[3]Mechanical, Biomedical and Design Engineering Department, School of Engineering and Technology, Aston University, England.
[4]Department of Mechanical Engineering, CECOS University of IT and Emerging Science, Peshawar, Pakistan

ATICLE INFO

Received: 19 Mar. 2021;
Received in revised form:
10 Oct. 2021;
Accepted: 10 Oct. 2021;
Published online:
14 Oct. 2021

Keywords:
Turbine
Empirical model
Mass flow rate
Isentropic Efficiency
Mean value model

ABSTRACT

Cavitation damage in centrifugal pump transporting slurry in a process industry has been investigated, quantified, and optimized for enhanced performance. The design of the experiment (DOE) method is used to generate 31 distinct impeller geometries to construct a mathematical relationship. Two objective functions, a net positive suction head (NPSHr) and pump efficiency (η), are employed to minimize and maximize the results through a quadratic regression model, respectively. The optimization technique is incorporated through a non-sorting genetic algorithm (NSGA-II). Rayleigh-Plesset cavitation model is utilized to compute the cavitation along with the SST turbulence model. Cavitation model validation is achieved through ALE-15 hydrofoil geometry. The simulation results agree well with the experimental data. A significant reduction of 12.6 % in NPSHr and an increase of 3.18% efficiency are achieved compared with the base design. A suction head (1.15 m) and a vapor pressure head (1.05 m) are identified as the threshold values for cavitation rate and efficiency. The current study will be beneficial for pump designers to adjust the geometric parameters at the preliminary stage to avoid substantial economic losses during the operational phase.

1. Introduction

Pumping system plays an imperative role in process industries for the transportation of liquids for small and medium distance applications. For this purpose, centrifugal pumps are usually employed. Moreover, to maintain uniform production levels, proper working of the transport equipment is mandatory [1]. Centrifugal pump handles the slurry transport successfully, however, it faces severe problem of cavitation at low pressure regions near impeller eye and on the blade surfaces. The bubble formation and burst due to implosion generate shock waves, which travel through the liquid and strike the impeller

*Corresponding e-mail: m.siddiqi5@aston.ac.uk (M. Siddiqi)

eye, and blades results in surface degradation. Wear due to cavitation is a complicated

b_1	inlet blade height	y+	dimensionless distance from 1st cell node
b_2	exit blade height	Δy	first layer thickness
$\sum h_L$	summation of all head losses		
m_{cav}	mass flowrate of cavitation bubble		
g	gravity		
k	turbulent kinetic energy		
Q	volume flowrate	*Abbreviations*	
S	shear stress	CCD	central composite design
F_2	blending function	ELM	energy loss model
F_{cond}	condensation empirical factor	SKE	simulation-Kriging model-Experiment
F_{vap}	vaporization empirical factor	MOO	multi-objective optimization
Hs	suction head	NPSH	net positive suction head
Hv	vapor pressure head	*Greek letters*	
L	characteristic length	β_1	turbine inlet
P	local pressure	β_2	blade outlet,
P_1	pressure at inlet	ɣ	specific weight
P_{min}	minimum pressure	ω	turbulent frequency
Pv	liquid vapor pressure	ρ	pure water density
		ρ_p	density of particle
r_1	impeller hub radius	ρ_f	density of liquid
r_2	impeller shroud radius	ρ_m	mixture density
r_f	radius of slurry droplet	α	regression coefficients for NPSHr
r_{nuc}	volume fraction of nucleation site	γ	regression coefficients for efficiency
r_p	radius of particle	σ	cavitation number
R_B	nucleation site radius	μ_m	mixture density
Re_L	Reynolds number		
T_∞	free stream temperature		
ui	x-component of velocity		
uj	y-component of velocity		
v	velocity		

phenomenon in centrifugal pumps and it involves surface damage and efficiency losses . Investigators have performed numerous experimental studies to examine cavitation in centrifugal pumps. Effect of surface topography, operating conditions, type of fluid on cavitation intensity is focused mostly. Drop in efficiency and performance deterioration are hardly addressed in the literature. Rao and Buckley et al.[2] investigated the effect of cavitation erosion in three distinct liquids, a viscous mineral oil, distilled water and ordinary tap water on aluminum 6061-T6. Obaid et al. [3] identified that the cavitation phenomenon in centrifugal pumps is dependent on different operating conditions like rotational speeds and different flow rates by utilizing the vibration technique. Mousmoulis et al.[4] studied cavitation in three different impellers of a laboratory centrifugal pump with a plexiglas casing, using flow visualization, vibration and acoustic emission measurements. Moreover, an experimental technique for analyzing the effect of blade geometry is developed for observing cavitation growth.

To study the different stages and forms of cavitation wear, latest computational techniques have been employed by the researchers. However, quantification and minimization of this undesirable phenomenon have rarely discussed. Rossetti et al.[5] performed 3D transient CFD simulations and validated the results through experimental data for first stage rotary shaft pump and second stage centrifugal viscous pump. Azizi et al.[6] presented a system for detection of cavitation severity in centrifugal pumps and for the improvement in its accuracy using a hybrid feature selection technique. A generalized regression neural network (GRNN) is used for cavitation identification. Ye et al.[7] investigated the cavitation phenomenon in a centrifugal pump through visualization experiments at different flow rates. Comparison between experimental and semi-analytical model is made for the pump head, cavity lengths and vapor volume fraction. Deng et al.[8] employed Zwart–Gerber–Belamri Model to predict and compare the vapor volume fraction between diesel and water liquids. Effects from viscosity and surface tension on bubbles' explosion and implosion are taken into account in the improved model rather than the traditional assumptions in which the bubble radius is just a function of pressure and density.

From last few years, optimization techniques have gain importance for geometric and flow optimization regarding the pump performance enhancement in various studies. Heo et al.[9] conducted a design optimization study for a centrifugal pump having backward-curved blades with a specific speed of 150, efficiency and total pressure have been taken as the objective functions. They have employed various surrogate models coupled with 3-D RANS analysis to investigate the performance characteristics of the centrifugal pump. Long et al. [10] conducted study to optimize the design of a typical multistage centrifugal pump based on energy loss model and Computational Fluid Dynamics (ELM/CFD). They have reduced the volumetric and inter-stage leakage losses to increase the efficiency of centrifugal pumps. Olszewski et al.[11] discussed the methodology for optimizing analysis of a complex pumping system with a set of parallel centrifugal pumps. They have tried to minimize power consumption and maximize the overall efficiency. Zheng et al. [12] proposed the multi-objective optimization method for a family of double suction centrifugal pumps with various blade shapes using a Simulation-Kriging model-Experiment (SKE) approach.

In most of the studies conducted by various researchers to address cavitation phenomenon, the focus seems to be on the inception, formation, reduction and types of cavitation. However, quantification of damage caused by this unwanted phenomenon is rarely considered. In the current study, cavitation in centrifugal pump transporting slurry in a process industry is investigated, quantified and minimized for better pump performance.

2. Theoretical aspects and governing equations

In the present work, a real cavitation problem is analyzed for a process industry. Centrifugal pumps are installed at Imperial Chemical Industries (ICI) located in Khewra, District Jhelum, Pakistan to transport slurry in soda ash production process. Pump impellers are damaged due to cavitation phenomenon occurring at impeller eye and blade locations as shown in (Fig. 1). Slurry contains calcium carbonate particles, which reacts and mixes with water to make it homogeneous slurry.

Fig. 1. Damaged centrifugal pump impellers due to cavitation

Due to this damage, pump impellers are replaced after almost every 6 months to keep running the plant operations smoothly. Some basic and important data obtained from industry pertinent to centrifugal pump, fluid and pumping system is listed in Table 1.

Table 1
Basic centrifugal pump data obtained from industry

Parameters	Description
Lime slurry	working fluid
Slurry density	1281 kg/ m3
Rated flow rate	120 m3/h
Pump efficiency	76.1 %
Pump NPSHr	3.73 m
Slurry temperature	50 – 90°C
Material of volute casing	Grey cast iron
Suction head	1.26 m
Discharge head	10.6 m
Impeller type	Semi-open impeller
Blade inlet height	4.56 cm
Blade inlet angle	28.5°
Blade exit height	3.31 cm
Blade exit angle	21.5°

2.1 Governing equations

Reynolds-Averaged-Navier-Stokes equations (RANS) are used to solve the fluid flow problem. Finite volume method is employed to solve these equations. Interested reader can found details in literature [13, 14].

2.1.1 Conservation and transport equations

The governing equations are the continuity, momentum and transport equations for the fluid flow, which is turbulent in nature, where two phases (slurry and vapor) behaves as a homogeneous mixture and share the same velocity and pressure fields.
Continuity equation:

$$\frac{\partial \rho_m}{\partial t} + \frac{\partial \left(\rho u_j\right)}{\partial x_j} = 0 \qquad (1)$$

Momentum conservation equation:

$$\frac{\partial \left(\rho u_i u_j\right)}{\partial x_j} = -\frac{\partial p}{\partial x_i} + \frac{\partial}{\partial x_j}\left[\left(\mu + \mu_t\right)\left(\frac{\partial u_i}{\partial x_j} + \frac{\partial u_j}{\partial x_i} - \frac{2}{3}\frac{\partial u_k}{\partial x_k}\delta_{ij}\right)\right]$$

2)
The slurry-vapor mass transport due to cavitation controlled by the vapor volume fraction transport is stated by the following equation:

$$\frac{\partial \left(\alpha_v \rho_v\right)}{\partial t} + \frac{\partial \left(\alpha_v \rho_v v_j\right)}{\partial x_j} = R_e - R_c \qquad (3)$$

The mixture density ρm and the mixture dynamic viscosity μm are given as:

$$\rho_m = \rho_v \alpha_v + \rho_l\left(1-\alpha_v\right) \qquad (4)$$

$$\mu_m = \mu_v \alpha_v + \mu_l\left(1-\alpha_v\right) \qquad (5)$$

2.1.2 Cavitation model

The cavitation growth rate of a vapor bubble in a liquid is governed by Rayleigh-Plesset model equation. This equation is used as a homogeneous mass transfer model in the multiphase framework and is applied to predict the cavitation rate.

$$R_B \frac{d^2 R_B}{dt^2} + 1.5\left(\frac{dR_B}{dt}\right)^2 + \frac{2\sigma}{\rho_f R_B} = \frac{p_v}{\rho_f} \qquad (6)$$

Eq. (6) is simplified by assuming surface tension and second order terms as negligible. The final expression has been obtained considering growth of vapor bubble and condensation as follows:

$$\dot{m}_{cav} = -F_e \frac{3 r_{nuc}\left(1-\alpha\right)\rho_v}{R_B}\sqrt{\frac{2}{3}\frac{p_v - p}{\rho_l}} \qquad (7) \text{ if } p<pv$$

$$\dot{m}_{cav} = F_c \frac{3\alpha\rho_v}{R_B}\sqrt{\frac{2}{3}\frac{P - P_v}{\rho_l}} \qquad (8) \text{ If } p>pv$$

Values of these parameters are shown in Table 2. ANSYS CFX [15] solver theory deals with the thorough explanation of multiphase models. Eq. (7) is used to estimate the cavitation rate through CFX expression language (CEL).

Table 2
Rayleigh-Plesset cavitation model parameters

Parameter	Value
Ps	2350 Pa

Fc	0.01
Fe	50
ρr	1000
rnuc	5e-4
Rf	0.25
RB	1 μm

2.2 Net positive suction head

Two values of NPSH are used. A required NPSH, denoted by NPSHr and the other one is available NPSH, written as NPSHA. NPSHA is a function of pumping system, must be calculated, whereas NPSHr is a function of the pump, and must be provided by the pump manufacturer. Put another way, you must have more suction side pressure available than the pump requires. The expressions for both of them are given in Eqs. (9) and (10).

$$NPSH_A = \frac{p_{atm}}{\gamma} - H_s - \sum h_L - H_v \quad (9)$$

$$NPSH_r = \frac{P_1 - P_{min}}{\rho g} + \frac{V_1^2}{2g} \quad (10)$$

Here, γ is the specific weight, Hs is the suction head, $\sum h_L$ is the summation of all head losses and pv is the liquid vapor pressure.
To avoid cavitation NPSHA > NPSHr. In order to evaluate the NPSHA, the parameters such as suction head, head losses due to friction and bends, vapor pressure head etc. are known. During the pump operation the NPSHA are decreased due to aforementioned parameters and are not in control as the process in industry doesn't allow to change the operating conditions. However, the geometry modifications can be made for safe operation of centrifugal pump and are favorable for minimizing the NPSHr.

2.3 Centrifugal pump parameters

Centrifugal pumps are the most commonly used radial pumps today. In current study, semi-open impeller centrifugal pump with backward curved blades is employed.

2.3.1 Pump efficiency

It is ratio of power actually gained by the fluid to the shaft power and is affected by three type of losses, i.e.; the hydraulic, mechanical, and the volumetric losses. Pump efficiency can be defined in terms of power [16]:

$$\eta = \frac{\rho g h_a Q}{W_{shaft}} \quad (11)$$

Or in terms of heads:

$$\eta = \frac{h_a}{h_i} \quad (12)$$

Eq. (11) is evaluated to get the pump efficiency values through CFX expression language (CEL) against different operating parameters. Here, Ps is shaft power, ρ is the slurry density, g is gravity, Q is the slurry volume flow rate, ha is actual head rise, hi is the ideal head rise and η is the pump efficiency.

2.3.2 Velocity triangles

Actually the flow through a pump is very complicated (unsteady and 3-D), the basic theory of centrifugal pump operation can be established by assuming the average 1-D flow of the fluid as it passes between the inlet and the exit sections of the impeller as the blades rotate. (Fig. 2) shows the velocity triangles utilized for the evaluation of various geometric parameters; such as impeller blade inlet and exit heights and blade angles, which are taken as design variables for optimization purpose in the current study.

$$V_{r2} = \frac{Q}{2\pi r_2 b_2} \quad (13)$$

The angle between the absolute velocity and the circumferential direction is 90, here, $(V_{\theta 1} = 0)$, therefore, V1 is a function of b1 or β1 as given in Eq. (14):

$$V_1 = V_{r1} = \frac{Q}{2\pi r_1 b_1} = \frac{U_1}{\cot\beta_1} \quad (14)$$

Moreover, the tangential component of absolute velocity is dependent on β2 as shown in Eq. (15):

$$V_{\theta 2} = U_2 - V_{r2}\cot\beta_2 \quad (15)$$

3. Details of Computational Approach

CFD analysis contains three basic steps; creation of computational model, mesh

generation and setting up of simulation procedure [17]. The details of each step are given in the subsequent subsections.

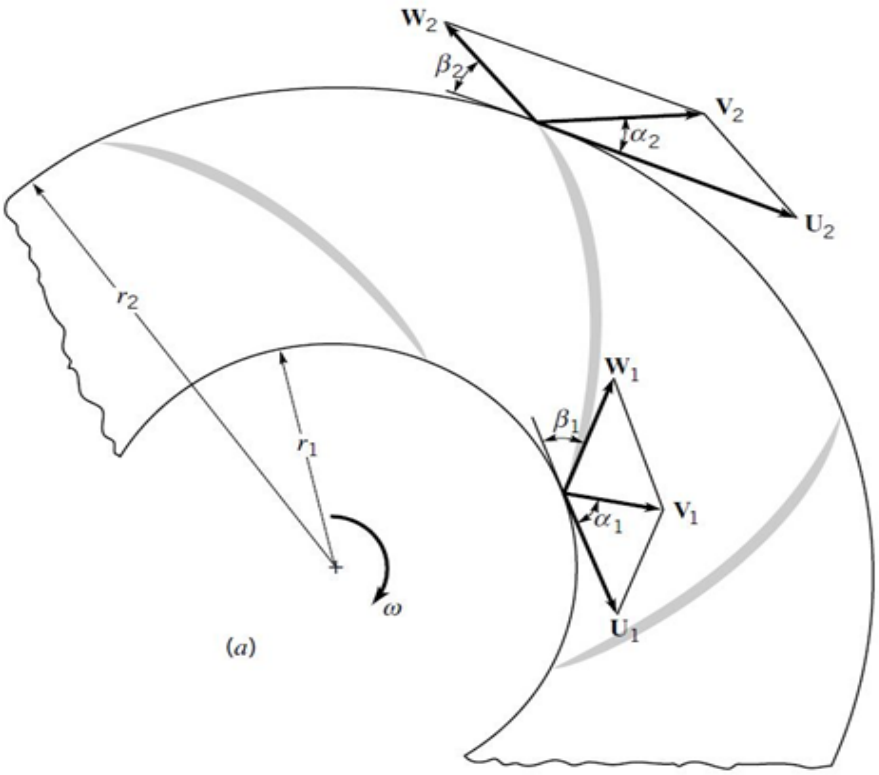

Fig.2. Velocity triangles for centrifugal pump impeller at the inlet and exit

3.1 Physical domain

The centrifugal pump is composed of two major parts; the volute casing and semi-open impeller. Design Modeler package is used to develop volute casing and impeller blades geometry. The blade profiles are generated through BladeGen module of ANSYS. The complete 3-D computational domain is shown in (Fig. 3).

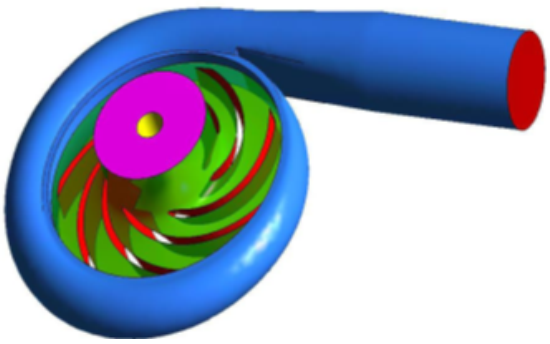

Fig. 3. Centrifugal pump computational domain

3.2 Mesh independence study

The whole domain has been meshed separately for both parts as shown in (Fig. 4 a); volute casing is meshed through CFX mesh module using unstructured mesh option which and is a good choice for intricate geometries as it provides higher flexibility for mesh generation. It contains hexahedral, prism and tetrahedral elements [18]. Body sizing along with inflation option has been applied near the surface of volute casing where the impeller

blades are attached as given in (Fig. 4 b). The impeller blades are meshed in Turbo Grid module of ANSYS. Hexahedral elements are used with factor base option near the blade surface. Moreover, mesh topology shown in (Fig. 4 c) is optimized near the blade surface for accurate results.

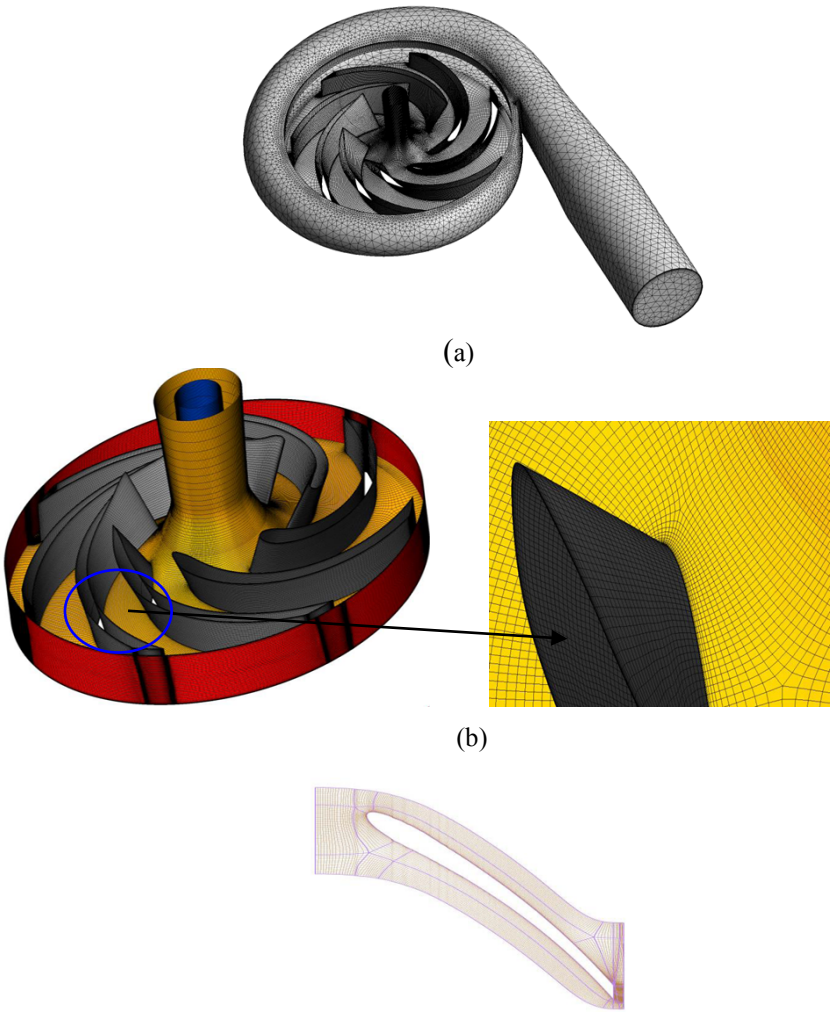

(a)

(b)

(c)

Fig. 4. Mesh details (a) whole domain, (b) inflation applied near blades

(c) Optimized topology around the blade

The accuracy of all the numerical solutions were found to be independent of the mesh used, which is accomplished by performing simulations with eight different meshes. Sensitivity of the solution is tested for each numerical mesh as given in (Fig. 5). For accurate and computationally economic solution a mesh size of 2.3 million elements is selected.

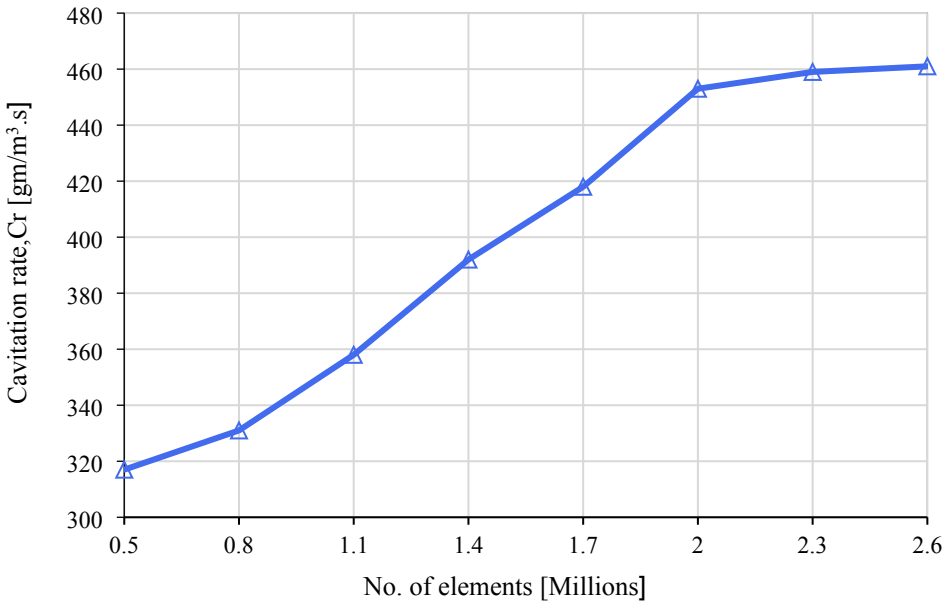

Fig. 5. Mesh sensitivity analysis

3.3 Turbulence modeling

To solve the boundary layer correctly and precisely, shear stress transport (SST) turbulence model is adopted which is a combination of k-ω (inside the boundary layer) and k-ε model (outside the boundary layer) and it takes care for the flow separation under adverse pressure gradients [8]. The y+ is estimated using Eq. (16). It is a dimensionless distance from the impeller blade wall surface to the first grid node, which comes out to around 6 for current problem [19].

$$\Delta y = L.y^{+}.\sqrt{74}.Re_{L}^{-13/14} \qquad (16)$$

where, Δy is the cell spacing, L is the characteristic length and ReL is the Reynolds number for the flow through impeller blades.

3.4 Simulation procedure

Continuity, momentum and transport equations are utilized and solved in ANSYS CFX solver. High resolution advection scheme has been employed to attain appropriate stability, convergence and accuracy. Mass flow rate at the inlet, static pressure at the outlet which changes with suction pressure variation and the no slip at the wall are the boundary conditions applied for the fluid domain. Fully developed profiles for velocity and pressure were introduced at the inlet and outlet respectively. The rotational speed of the impeller was taken as 1500 rpm [20]. In all the cases, steady state solution without cavitation was used as an initial results file for unsteady state calculation with cavitation. A low mass flow rate was primarily utilized for the flow domain, for which no vapor appears. The flow rate was then increased gradually till the rated flow was reached. Three full revolutions of the impeller were utilized to solve the transient case. Time step for the transient simulations

was estimated to be 1.1 x 10-4 s. For the cavitation case, the volume fraction of slurry and vapor were considered to be 0 and 1 respectively. The residual value for convergence is fixed at 10-5 of the initial value for mass and momentum variables.

4. Optimization Methodology

Optimization methodology utilized in the current study contains design of experiment (DOE) [21] for the proposed centrifugal pump geometry, which is employed to establish the regression model depending on the numerical results. Moreover, it serves as an objective function for an optimization procedure in terms of the design variables. The famous genetic algorithm (NSGA-II) is used for this purpose. However, DOE is the best suitable approach to manage different design variables having small measureable data [22]. Thus, DOE along with a NSGA-II was found appropriate for the present work.

4.1 Design of experiment technique

Several investigators have used DOE technique for the optimization of different problems in case of limited experimental/numerical data. Therefore, four design variables [24] have been opted for the optimization procedure along with the constraints as listed in Table 3.

Table 3. Four distinct design variables with constraints

Design variable	Symbol	Lower bound-Upper bound
Inlet blade angle [degree]	β_1	25-35
Exit blade angle [degree]	β_2	20-25
Inlet blade height [cm]	b_1	5.2-3.2
Exit blade height [cm]	b_2	3.8-2.3

Design variables and constraints were chosen based on the results of the earlier work [9, 21] to make sure that optimized values must fall within the permissible bounds. A quadratic regression model has been selected for the present work, which is shown in Eqs. (17 & 18) for dependent variables i.e.; required net positive suction head, $NPSH_r$ and pump efficiency η. Design of experiment with central composite design (CCD) technique is utilized, which facilitates the evaluation of metamodel and lead towards the selection of choices in optimal space-filling design. CCD is based on embedded 2^k factorial design with a set of star and central points. The relationship between the design variables and objective functions are chosen using a quadratic model given by

$$NPSH_r = \alpha_0 + \sum_{i=1}^{n} \alpha_i x_i + \sum_{i=1}^{n} \alpha_{i,i} x_i^2 + \sum_{i=1}^{n-1} \sum_{j=i+1}^{n} \alpha_{i,j} x_i x_j + \epsilon \quad (18)$$

$$\eta = \delta_0 + \sum_{i=1}^{n} \delta_i x_i + \sum_{i=1}^{n} \delta_{i,i} x_i^2 + \sum_{i=1}^{n-1} \sum_{j=i+1}^{n} \delta_{i,j} x_i x_j + \epsilon \quad (19)$$

$\alpha_0, \alpha_i, \alpha_{i,i}\ \alpha_{i,j}$ are regression coefficients, namely intercept, linear, quadratic and interaction for $NPSH_r$ the expression
$\delta_0, \delta_i, \delta_{i,i}\ \delta_{i,j}$ are regression coefficients, namely intercept, linear, quadratic and interaction for the η expression 31 distinct geometries have been created for centrifugal pump impeller, each DOE signifies a unique geometry design. The values of $NPSH_r$ and efficiency are evaluated through CFD and are listed in Table 4.

4.2 Genetic algorithm

It is a statistical tool that has often been utilized by the researchers working in various domains [25] for optimization studies. The genetic technique is dependent on the existence for the fittest principal. In previous studies, the genetic algorithm has been coupled with DOE [27] for design optimization work. Non-sorting genetic algorithm (NSGA-II) is employed in the current study. The process begins with defining the design variables and constraints. The population size is defined as 100, while crossover and mutation fraction are chosen as 0.8 and 0.2 respectively. Fitness

calculation was obtained through changes in the fitness function. A trade-off optimal solution is obtained through NSGA-II [27] which is based on single fitness measure for determining multiple objective.

Table 4. Blade design based on CDD for Cp performance enhancement

	b_1 [cm]	β_1 [degree]	b_2 [cm]	β_2 [degree]	$NPSH_r$	η
1	4.7	2.675	27.5	23.75	3.12	76.24
2	3.7	3.425	27.5	23.75	2.53	81.45
3	3.7	3.425	32.5	21.25	3.37	83.21
4	4.2	3.05	35	22.5	3.17	72.34
5	5.2	3.05	30	22.5	4.07	74.38
6	3.7	2.675	32.5	21.25	3.03	68.32
7	4.2	3.05	30	22.5	3.54	77.82
8	4.7	2.675	27.5	21.25	3.29	82.34
9	4.2	3.05	30	22.5	3.06	73.67
10	4.2	3.8	30	22.5	2.95	82.35
11	4.2	3.05	30	22.5	3.52	70.64
12	3.2	3.05	30	22.5	2.68	73.24
13	3.7	2.675	32.5	23.75	3.19	72.56
14	4.2	3.05	30	22.5	3.43	76.56
15	4.2	3.05	30	20	4.13	82.32
16	3.7	2.675	27.5	21.25	2.53	71.24
17	4.7	3.425	32.5	21.25	3.31	81.45
18	4.7	3.425	32.5	23.75	3.07	76.51
19	4.7	3.425	27.5	21.25	3.23	82.34
20	4.2	3.05	30	25	3.63	81.38
21	4.2	3.05	30	22.5	4.08	71.22
22	4.2	2.3	30	22.5	3.24	77.82
23	4.2	3.05	30	22.5	3.26	72.54
24	3.7	3.425	27.5	21.25	2.76	81.67
25	4.2	3.05	30	22.5	3.21	90.35
26	4.7	2.675	32.5	23.75	3.15	80.64
27	4.2	3.05	25	22.5	3.27	83.24
28	4.7	2.675	32.5	21.25	3.18	82.56
29	3.7	3.425	32.5	23.75	3.16	91.56
30	3.7	2.675	27.5	23.75	3.68	74.21
31	4.7	3.425	27.5	23.75	3.27	81.64

Termination criteria were selected depending on the function tolerance. Genetic algorithm application details are available for interested reader [33, 34].The detailed optimization process are listed in Table 5.

Table 5
Genetic algorithm parameters

Parameter	Value
Population size	100
Crossover fraction	0.8
Mutation fraction	0.2
Objective function tolerance	10-6
Selection function	tournament

Response surfaces of the required net positive suction head, NPSHr and efficiency, η were obtained as a function of design variables b1, β1, b2 and β2, and response surfaces are generated which are shown in (Figs. 7-8). The regression models are computed through DOE analysis and are given by the Eqs. (19) & (20). (Fig.6) shows a response surface of NPSHr bounded by the inlet bade height and inlet blade angle b1 and β1. The response surface shows that required net positive suction head exhibits a non-linear behavior with both the design variables. It is reduced with the decrease in both the inlet bade height (b1) and the value of the inlet blade angle (β1). However, efficiency increases with the higher value of inlet blade height and lower value of inlet blade angle. (Fig.7) presents a response surface of NPSHr bounded by the exit bade height and exit blade angle b2 and β2. The required net positive suction head is minimized with decrease in both the parameters. However, efficiency is maximized for higher values of both the parameters.

$$NPSH_r = -46.7 + 6.73b_1 + 7.47b_2 + 1.55\beta_1 + 0.07\beta_2 - 0.252b_1^2 - 0.945b_2^2 - 0.0163\beta_1^2 + 0.0405\beta_2^2 + 0.250b_1b_2 - 0.0725b_1\beta_1 - 0.127b_1\beta_2 + 0.0793b_2\beta_1 - 0.233b_2\beta_2 - 0.02222\beta_1\beta_2 \quad (19)$$

$$\eta = 342 + 146.6b_1 + 8.4b_2 - 9.4\beta_1 - 40.5\beta_2 - 1.73b_1^2 + 8.08b_2^2 + 0.090\beta_1^2 + 1.010\beta_2^2 - 17.13\,b_1b_2 - 0.42b_1\beta_1 - 2.90b_1\beta_2 + 0.37b_2\beta_1 + 0.44b_2\beta_2 + 0.196\beta_1\beta_2 \quad (20)$$

An optimization procedure can be employed for the desired results, once the expressions for the objective functions are known.

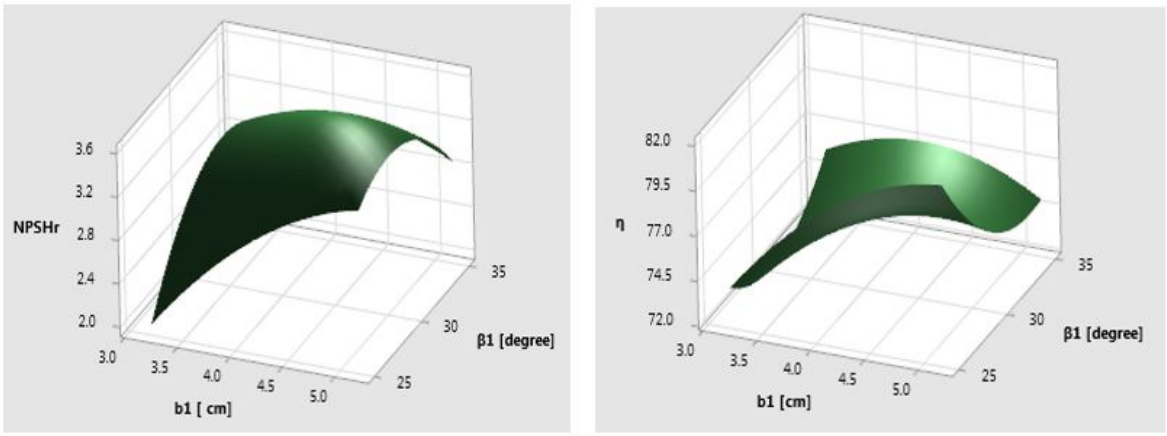

a) b)

Fig. 6. $NPSH_r$ and η response surfaces bound by geometrical parameters b_1 and β_1

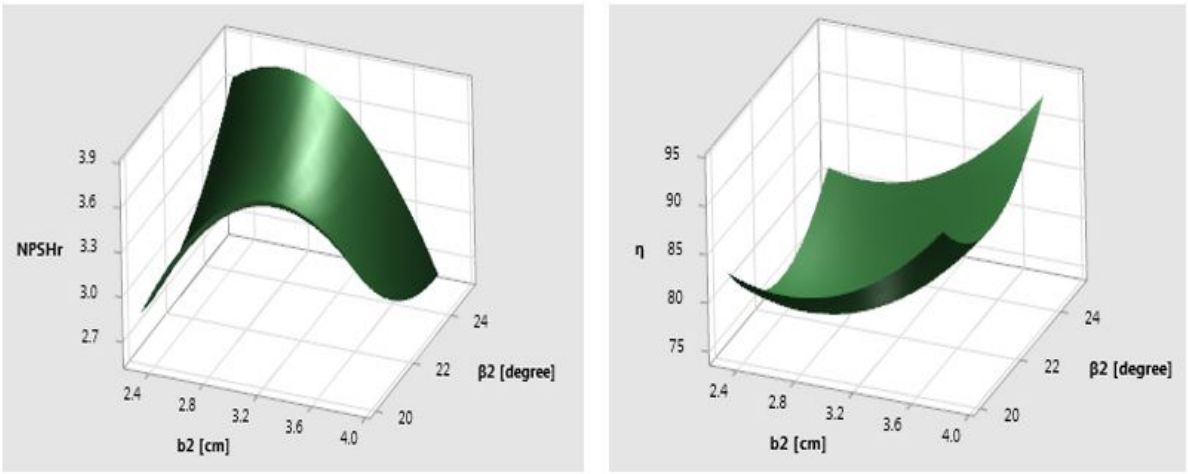

a) b)

Fig. 7. $NPSH_r$ and η response surfaces bound by geometrical parameters b_2 and β_2

5. Results and discussion

The performance enhancement of a centrifugal pump is achieved through an are compared with the base values for design variables and objective functions. A significant reduction of 12.6 % is achieved in NPSHr and optimization technique. Required net positive suction head, NPSHr is minimized and efficiency, η is maximized as the two objectives. The optimized values obtained an increase in efficiency of 3.18 % is obtained through optimization technique. The detailed comparison is shown in Table 6.

Table 6
Comparision of optimum values with the base values

Parameter	Symbol	Optimized value	Base value
Inlet blade height [cm]	b1	4.73	4.56
Inlet blade angle [degree]	β1	26.5	28.5
Exit blade height [cm]	b2	3.16	3.31
Exit blade angle [degree]	β2	22.5	21.5
Net positive suction head [m]	NPSHr	3.26	3.73
Efficiency [%]	η	78.6	76.1

5.1 Validation

A simple hydrofoil geometry is employed for validation purpose. Dular et al. [27] conducted an experimental work on a simple hydrofoil and tested it in a rectangular section in a water tunnel, whose dimensions are 500 mm in length, 50 mm wide and 100 mm high available at Darmstadt University of Technology. To obtain 3-D cavitation effects, asymmetric hydrofoil which is 107.9 mm long, having a span of 50 mm and 16 mm in thickness, with a slant or sweeping angle of 15º and an angle of attack as 5º is employed as presented in (Fig.8). The Rayleigh–Plesset equation is used to derive source terms, which are functions of local flow conditions (static pressure and velocity) and fluid properties (liquid and vapor phase densities, liquid and vapor phase viscosities and liquid vapor surface tension). Two models full cavitation model (FCM) and Zwart model are employed which are derived through Rayleigh-Plesset equation.. The properties utilized for liquid and vapor are given in Table 7.

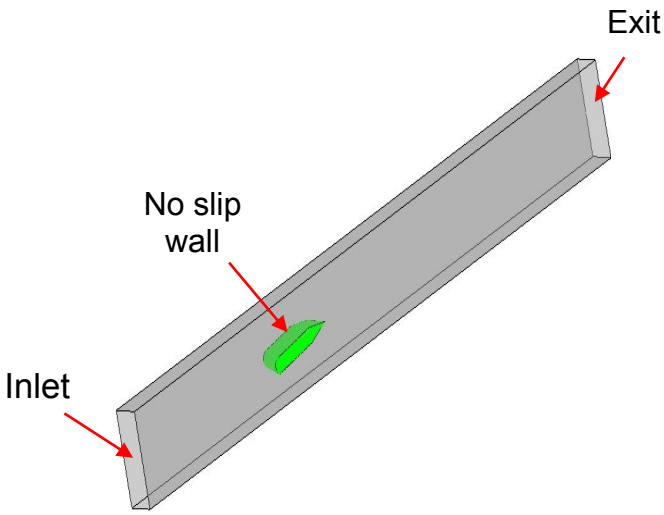

Fig. 9. 3-D view of the hydrofoil placed in a rectangular test section

Table 7
Details of liquid and vapor properties

Property	Symbol	Value with units
Liquid density	ρl	998.2 kg/m3
Vapor density	ρv	0.554 kg/m3
Liquid viscosity	μl	10−3 Pas
Vapor viscosity	μv	1.34 × 10−5 Pas
Surface tension	γ	0.0717 N/m
Gas mass fraction	fg	5 × 10−5

The artificial intelligence approaches are much closer to human thinking than traditional classical approaches. These methods mainly include artificial neural networks, fuzzy logic, and genetic algorithms. For turbines, the majority of these studies focused on artificial neural networks for health monitoring, diagnostics and prognostics. However, the application of the neural network method to modelling turbine performance maps is rare.
neural networks to model turbine performances.
Half O-Grid technique is used for the structured mesh creation in ANSYS ICEM. A fine mesh from leading edge through trailing edge is utilized near the hydrofoil surface as shown in (Fig. 9). Velocity at inlet and static pressure at exit of the hydrofoil are the boundary conditions applied. Free slip wall boundary condition is applied at the side, top and bottom walls and no slip boundary condition on the surface of hydrofoil. Compressibility effects were neglected. Pressure coefficient (Cp) and cavitation number are associated through equation 20. Cp is plotted against the various locations on the hydrofoil top surface as presented in (Fig. 11), which is defined as ratio of the pressure difference between local and vapor pressure to the dynamic pressure:

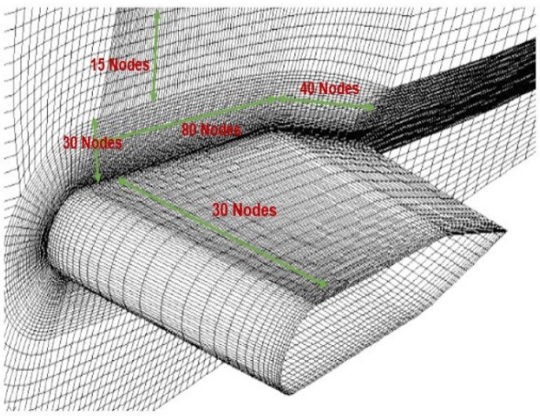

Fig. 9. ALE-15 hydrofoil mesh configuration

International Journal of Thermofluid Science and Technology (2021)
Volume 8, Issue 4, Paper No. 080404
https://doi.org/10.36963/IJTST.2021080404
Research Article

$$\sigma = -C_p = \frac{P - P_v(T)}{\frac{1}{2}\rho V^2} \qquad (22)$$

Cp is increased from leading edge to the trailing edge due to drop in the local pressure values on the hydrofoil surface. Two locations are highlighted to describe the Cp variation. Most of the Cp values are higher on line 21-25 than the middle line due to the attached cloud cavitation as shown in (Fig. 11). Both models showed the comparable trend with the tested results. The FCM cavitation model results are found to be closer to experimental ones with error of around 5%. Therefore, it is utilized for all the simulation cases.

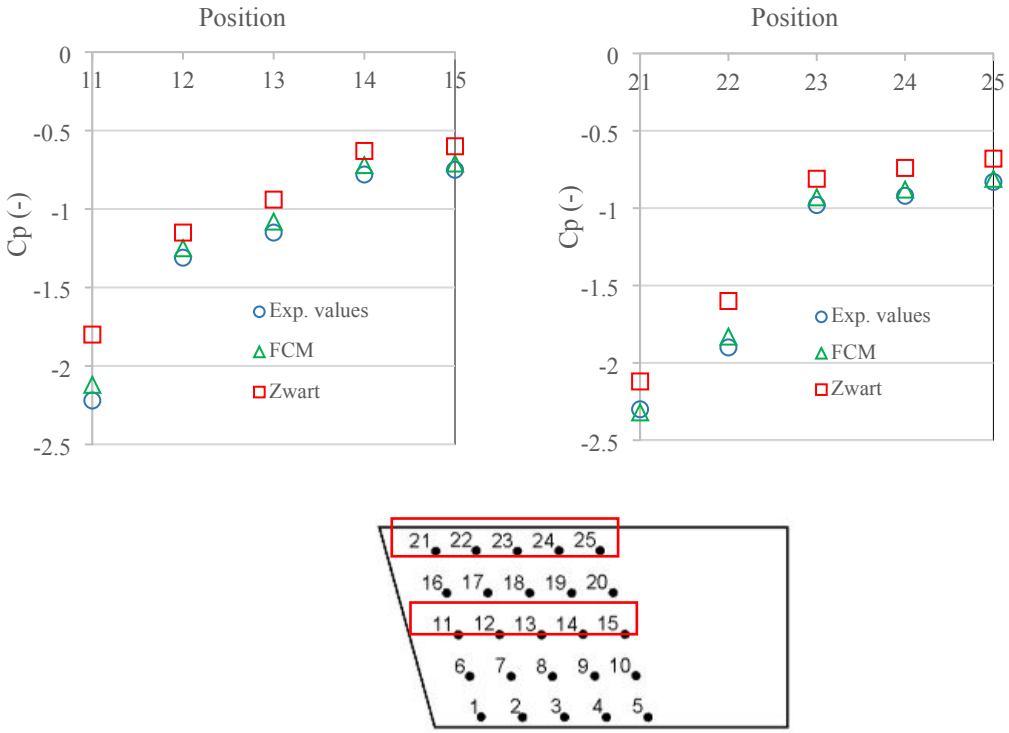

Fig. 11. Comparison of Zwart and FCM models with experimental Cp values at 2 distinct location

5.1 Performance enhancement

The performance of centrifugal pump can be enhanced through reduction in cavitation, which can be achieved by two different ways, i.e. by varying the flow conditions and modifying the impeller geometry. The former approach is not effective because varying the flow conditions disturbs the production process requirements and may affect the production capacity in the industry. The later approach seems useful by slightly changing the inlet and outlet blade heights and angles, which can help in reducing the cavitation damage without disturbing the plant process. Vapor volume fraction values are compared between optimized and base designs for slurry flow as given in (Fig. 12).

*Corresponding e-mail: m.siddiqi5@aston.ac.uk (M. Siddiqi)

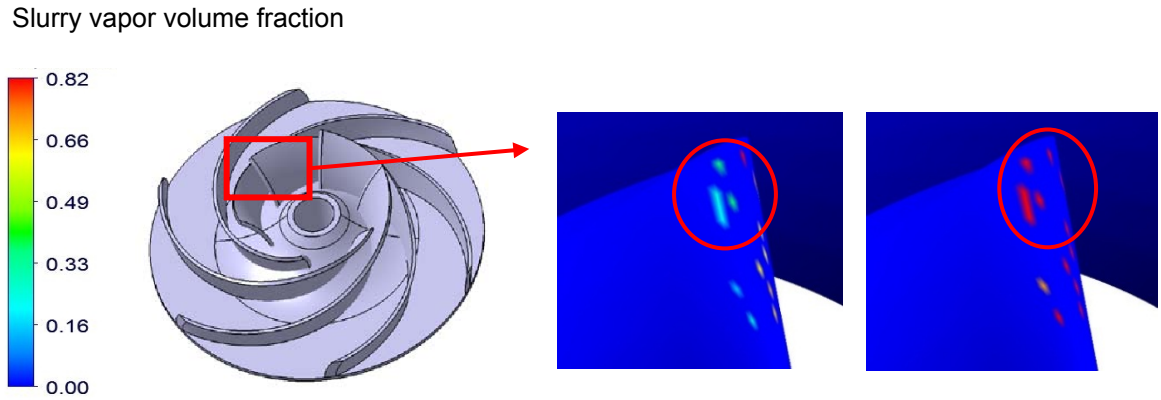

Fig.12. Slurry vapor volume fraction comparison between optimized and base designs for slurry

A wide range of suction head values (0.94 – 1.56 m) and vapor pressure head values (0.84 – 1.34 m); obtained from site are utilized to compare the optimized values with the base design ones for the purpose of performance enhancement. However, the higher values for both the suction and vapor pressure heads can be minimized by small adjustments such as to maintain the sump tank level uniform during the process and insulating the suction and delivery pipes, so that temperature of slurry not rise above 60.

5.1.1 Cavitation rate as a function of suction and vapor pressure heads

Cavitation rate, Cr increases with increase in suction head at a fixed vapor pressure head as presented in (Fig. 13 a). Optimized and base values are plotted for comparison. A linear variation with lower slope initially and higher after 1.15 m Hs value is found. However, the reduction in cavitation rate due to design optimization seems ineffective for higher values of suction head.

Cavitation rate, Cr increases with increase in vapor pressure head at a fixed suction head as presented in (Fig. 13 b). Optimized and base values are plotted for comparison. A very small rise in cavitation loss is observed initially, however slope increases rapidly between (1-1.1m) Hv values due to increase in slurry temperature. The reduction in cavitation rate due to design optimization seems effective until 1.05 m Hv value.

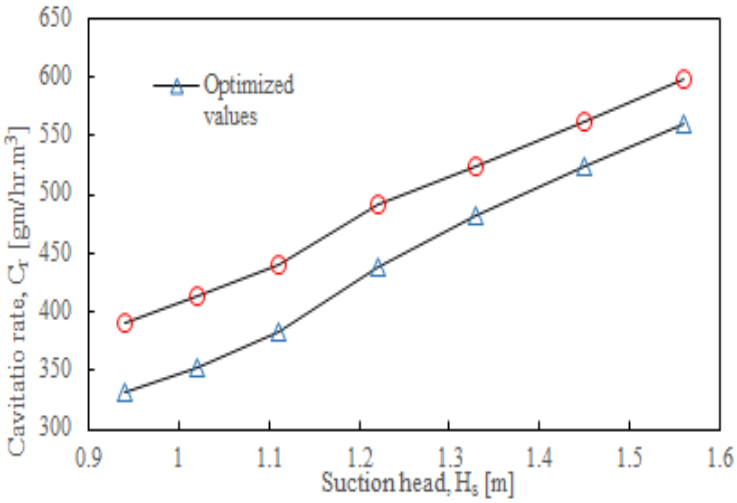

a)

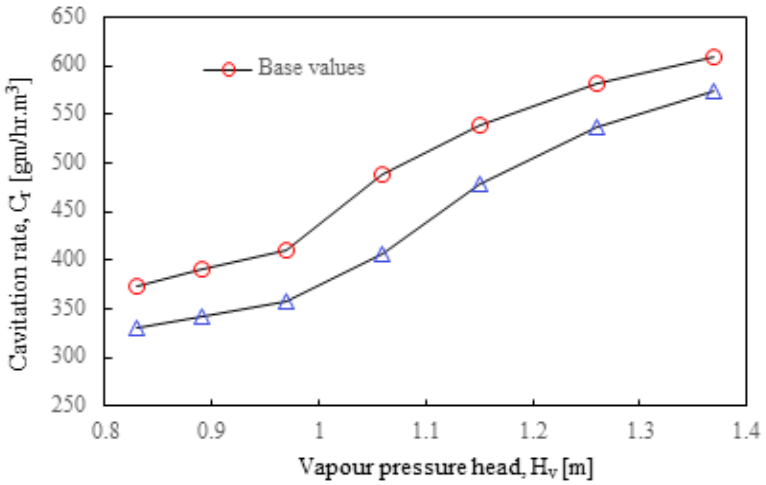

b)

Fig. 13. Comparison between optimized and base values for cavitation rate as a function of a) Suction head b) Vapor pressure head

5.1.2 Efficiency as a function of suction and vapor pressure heads

Efficiency decreases with increase in suction head at constant vapor pressure head as presented in (Fig. 14 a). Optimized and base values are plotted for comparison. Reduction in efficiency is slow initially; however, it decreases rapidly after 1.15 m Hs. As suction pressure is dependent on the process requirements and is not completely in the control of a system designer, a tradeoff between efficiency and suction head seems necessary. However, the optimized geometry helped in enhancement of pump efficiency around more than 2% Efficiency decreases almost linearly with increase in vapor pressure head at constant suction head as presented in (Fig. 14 b). Optimized and base values are plotted for comparison. As the process temperature fluctuates, the vapor pressure of the slurry increases which results in efficiency drop. The optimization of impeller blade geometry has assisted in enhancement of pump efficiency to around 2.5%.

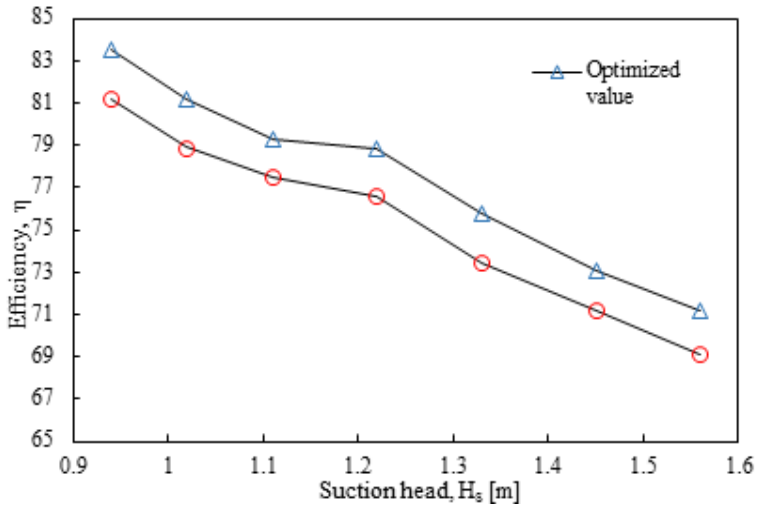

a)

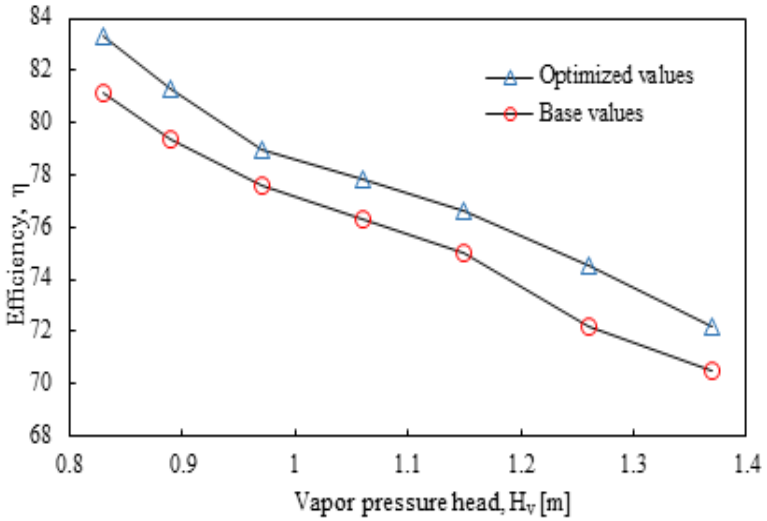

b)

Fig. 14. Comparison between optimized and base values for efficiency as a function of a) Suction head b) Vapor pressure head

6. Conclusion

Cavitation in centrifugal pump transporting lime slurry has been investigated numerically. The optimization study based on DOE has been conducted to minimize the net positive suction head (NPSHr) and maximize the pump efficiency (η) as the two objective functions. The parametric data is collected from 31 different geometries of impeller. Following conclusions are drawn from the current work:

- 1.15 m and 1.05 m suction and vapor pressure heads, respectively, are identified as the threshold values corresponding to cavitation rate and pump efficiency.
- The aforementioned values of suction and vapor pressure heads can be achieved by maintaining the sump tank level uniform during the process and insulating the suction and delivery pipes.
- A substantial reduction of 12.6 % in NPSHr and an increase of 3.18 % in efficiency are obtained through the geometrical optimization as compared with the base design.
- Design of experiment (DOE) technique based on regression models is developed and coupled with NSGA-II for geometry optimization, which minimized the lengthy computational time.
- Surface roughness effects will be taken into account that would furnish more accurate results for the cavitation damage. Additionally, the correlations will be developed for cavitation rate as a function of suction, vapor pressure heads and surface roughness.

References

1. Rao, P.V. and D.H. Buckley, Predictive capability of long-term cavitation and liquid impingement erosion models. Wear, 1984. 94(3): p. 259-274.
2. Rao, B. and D. Buckley, Erosion of aluminum 6061-T6 under cavitation

attack in mineral oil and water. Wear, 1985. 105(2): p. 171-182.
3. Al-Obaidi, A.R., Investigation of effect of pump rotational speed on performance and detection of cavitation within a centrifugal pump using vibration analysis. Heliyon, 2019. 5(6): p. e01910.
4. Mousmoulis, G., et al., Experimental analysis of cavitation in a centrifugal pump using acoustic emission, vibration measurements and flow visualization. European Journal of Mechanics-B/Fluids, 2019. 75: p. 300-311.
5. Rossetti, A., G. Pavesi, and G. Ardizzon, A new two stage miniature pump: Design, experimental characterization and numerical analyses. Sensors and Actuators A: Physical, 2010. 164(1-2): p. 74-87.
6. Azizi, R., et al., Improving accuracy of cavitation severity detection in centrifugal pumps using a hybrid feature selection technique. Measurement, 2017. 108: p. 9-17.
7. Ye, Y., et al., Application of the semi-analytical cavitation model to flows in a centrifugal pump. International Communications in Heat and Mass Transfer, 2017. 86: p. 92-100.
8. Deng, S.-S., et al., Numerical study of cavitation in centrifugal pump conveying different liquid materials. Results in Physics, 2019. 12: p. 1834-1839.
9. Heo, M.-W., et al., High-efficiency design optimization of a centrifugal pump. Journal of Mechanical Science and Technology, 2016. 30(9): p. 3917-3927.
10. Long, X., et al., Experimental investigation on the performance of jet pump cavitation reactor at different area ratios. Experimental Thermal and Fluid Science, 2016. 78: p. 309-321.
11. Olszewski, P., Genetic optimization and experimental verification of complex parallel pumping station with centrifugal pumps. Applied Energy, 2016. 178: p. 527-539.
12. Zhang, Y., et al., Multi-objective optimization of double suction centrifugal pump using Kriging metamodels. Advances in Engineering Software, 2014. 74: p. 16-26.
13. Amarendra, H., G. Chaudhari, and S. Nath, Synergy of cavitation and slurry erosion in the slurry pot tester. Wear, 2012. 290: p. 25-31.
14. Salim, S.M. and S. Cheah. Wall Y strategy for dealing with wall-bounded turbulent flows. in Proceedings of the international multiconference of engineers and computer scientists. 2009.
15. Xie, J., et al., A numerical prediction on heat transfer characteristics from a circular tube in supercritical fluid crossflow. Applied Thermal Engineering, 2019. 153: p. 692-703.
16. Gohil, P.P. and R. Saini, Effect of temperature, suction head and flow velocity on cavitation in a Francis turbine of small hydro power plant. Energy, 2015. 93: p. 613-624.
17. Shoukat, A.A., et al., Blades Optimization for Maximum Power Output of Vertical Axis Wind Turbine. 2021. 10(3).
18. Noon, A.A. and M.-H. Kim, Erosion wear on centrifugal pump casing due to slurry flow. Wear, 2016. 364: p. 103-111.
19. Vojtáš, P. and M. Vomlelová, Learning Fuzzy Logic Aggregation for Multicriterial Querying With User Preferences. LINZ, 2006: p. 128.
20. Wang, Z., et al., Effects of flow rate and rotational speed on pressure fluctuations in a double-suction centrifugal pump. Energy, 2019. 170: p. 212-227.
21. Pei, J., W. Wang, and S. Yuan, Multi-point optimization on meridional shape of a centrifugal pump impeller for performance improvement. Journal of Mechanical Science and Technology, 2016. 30(11): p. 4949-4960.
22. Lomakin, V., P. Chaburko, and M. Kuleshova, Multi-criteria optimization

of the flow of a centrifugal pump on energy and vibroacoustic characteristics. Procedia Engineering, 2017. 176: p. 476-482.
23. Ding, H., et al., The influence of blade outlet angle on the performance of centrifugal pump with high specific speed. Vacuum, 2019. 159: p. 239-246.
24. Reeves, C.R., Genetic algorithms, in Handbook of metaheuristics. 2010, Springer. p. 109-139.
25. Fang, X., et al., Research on improved NSGA-II algorithm and its application in emergency management. Mathematical Problems in Engineering, 2018. 2018.
26. Cody, B.M., Application of semi-analytical multiphase flow models for the simulation and optimization of geological carbon sequestration. 2014, Colorado State University.
27. Dular, M., et al., Experimental evaluation of numerical simulation of cavitating flow around hydrofoil. European Journal of Mechanics-B/Fluids, 2005. 24(4): p. 522-538.